# Periodic sticking motion in a two-degree-of-freedom impact oscillator

David J Wagg

▶ **To cite this version:**

David J Wagg. Periodic sticking motion in a two-degree-of-freedom impact oscillator. International Journal of Non-Linear Mechanics, 2005, 40 (8), pp.1076-1087. 10.1016/j.ijnonlinmec.2005.03.002 . hal-01509345

**HAL Id: hal-01509345**
**https://hal.science/hal-01509345**

Submitted on 17 Apr 2017

**HAL** is a multi-disciplinary open access archive for the deposit and dissemination of scientific research documents, whether they are published or not. The documents may come from teaching and research institutions in France or abroad, or from public or private research centers.

L'archive ouverte pluridisciplinaire **HAL**, est destinée au dépôt et à la diffusion de documents scientifiques de niveau recherche, publiés ou non, émanant des établissements d'enseignement et de recherche français ou étrangers, des laboratoires publics ou privés.

Distributed under a Creative Commons Attribution 4.0 International License

# Periodic sticking motion in a two-degree-of-freedom impact oscillator

D.J. Wagg

*Department of Mechanical Engineering, University of Bristol, Queens Building, University Walk, Bristol BS8 1TR, UK*

Periodic sticking motions can occur in vibro-impact systems for certain parameter ranges. When the coefficient of restitution is low (or zero), the range of periodic sticking motions can become large. In this work the dynamics of periodic sticking orbits with both zero and non-zero coefficient of restitution are considered. The dynamics of the periodic orbit is simulated as the forcing frequency of the system is varied. In particular, the loci of Poincaré fixed points in the sticking plane are computed as the forcing frequency of the system is varied. For zero coefficient of restitution, the size of the sticking region for a particular choice of parameters appears to be maximized. We consider this idea by computing the sticking region for zero and non-zero coefficient of restitution values. It has been shown that periodic sticking orbits can bifurcate via the rising/multi-sliding bifurcation. In the final part of this paper, we describe three types of post-bifurcation behavior which occur for the zero coefficient of restitution case. This includes two types of rising bifurcation and a border orbit crossing event.

*Keywords:* Impact; 2DOF Oscillator; Periodic; Sticking; Multi-sliding

## 1. Introduction

In this paper periodic sticking motions which occur in the dynamics of a two-degree-of-freedom impact oscillator are considered. The impact oscillator consists of two masses, coupled with springs and dashpots, and the motion of both the masses is restricted by rigid constraints [1]. These type of systems can be used to model a range of physical applications mainly in mechanical engineering [2–9]. Many mathematical–numerical studies of these systems have been carried out, and particular interest has been focused on bifurcation behavior [10–16]. More general studies of multiple degree of freedom impact oscillators have also been carried out [17–22], but these focus primarily on a single impact constraint.

In mechanical systems with vibration and impact, chatter and sticking are phenomena which have been observed for a wide range of parameter values. Chatter and sticking in single degree of freedom impact oscillators has been studied in detail [23,24] and also noted

to occur in two-degree-of-freedom systems, particularly for low forcing frequencies [25]. Vibro-impact systems exhibit a rich variety of periodic motions (see for example [26]), and periodic sticking motions can be found for particular parameter values in both single and multi-degree-of-freedom systems. Multi-degree-of-freedom systems with a single constraint have been studied by Toulemonde and Gontier [27] and Wagg and Bishop [25], where periodic sticking motions were observed for low forcing frequencies. In [1], periodic sticking motions were noted for a two-degree-of-freedom impact oscillator with two constraints, and it was shown how the entry boundary to the sticking region can be defined. The rising bifurcation discussed by Toulemonde and Gontier [27] has been shown to be equivalent to the multi-sliding bifurcation [28], which occurs in the study of nonsmooth systems [29–31].

In this paper, we study the dynamics of periodic sticking motions which exist in a two-degree-of-freedom impact oscillator with motion constraints on both masses [1]. For low (or zero) coefficient of restitution, the range of periodic sticking motions becomes large. This is significant because the maximum extent of the sticking region should be defined for the zero case. This idea is considered by using a comparison of the sticking region obtained by simulating the dynamics of periodic sticking orbits with both zero and non-zero coefficient of restitution. Then the loci of Poincaré fixed points in the sticking plane are computed as the forcing frequency of the system is varied. Projections of these loci into the system state space indicate that the zero case does not define the largest region of sticking motions for the examples considered.

In the final part of this paper, we consider the post-bifurcation behavior following rising bifurcations in the zero coefficient of restitution case. We first illustrate the 'standard' rising bifurcation behavior described by Wagg and Bishop [1,27] and following this we describe one other example where the rising has a receding behavior. Finally we discuss an example were a sticking orbit passes through a border orbit [24], which defines the limiting extent of the sticking region.

## 2. Mathematical model

We consider a coupled two-degree-of-freedom system, which is shown schematically in Fig. 1. This system has already been described in detail in [1,28]. The governing equations for the system away from impact can be expressed as

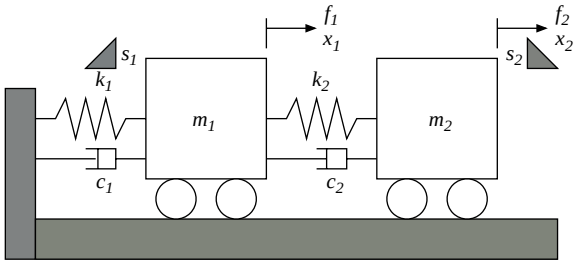


Fig. 1. Schematic representation of an $N$ degree of freedom impact oscillator with multiple motion limiting constraints.

$$m_1\ddot{x}_1 + c_1\dot{x}_1 + c_2(\dot{x}_1 - \dot{x}_2) + k_1x_1 + k_2(x_1 - x_2) = f_1, \tag{1}$$

$$m_2\ddot{x}_2 + c_2(\dot{x}_2 - \dot{x}_1) + k_2(x_2 - x_1) = f_2, \tag{2}$$

where $x_1$ represents the displacement of mass $m_1$ and $x_2$ the displacement of mass $m_2$. The spring stiffnesses are given by $k_1$, $k_2$ and the damping constants by $c_1$, $c_2$ and the distance to the motion constraints are given by $s_1$ and $s_2$, respectively. The harmonic forcing functions are $f_1 = A_1\cos(\Omega t)$ and $f_2 = A_2\cos(\Omega t)$. Eq. (2) has a dual condition for free flight that $(x_i - s_i) < 0$ for $s_i > 0$ and $(x_i - s_i) > 0$ for $s_i < 0$ which can be written as $(x_i - s_i) \lesseqgtr 0\ \forall s_i \gtreqless 0$ for $i = 1, 2$. We also assume that the distance between masses is large enough so that they do not impact with each other.

Eqs. (1) and (2) can be written in the non-dimensionalized form

$$\begin{bmatrix} \mu_m & 0 \\ 0 & 1 \end{bmatrix}\begin{bmatrix} \ddot{\xi}_1 \\ \ddot{\xi}_2 \end{bmatrix} + \begin{bmatrix} 2\zeta_1\sqrt{\mu_m\mu_k} + 2\zeta_2 & -2\zeta_2 \\ -2\zeta_2 & 2\zeta_2 \end{bmatrix}\begin{bmatrix} \dot{\xi}_1 \\ \dot{\xi}_2 \end{bmatrix} + \begin{bmatrix} 1+\mu_k & -1 \\ -1 & 1 \end{bmatrix}\begin{bmatrix} \xi_1 \\ \xi_2 \end{bmatrix} = \begin{bmatrix} \tilde{f}_1 \\ \tilde{f}_2 \end{bmatrix}, \tag{3}$$

where $\mu_m = m_1/m_2$, $\mu_k = k_1/k_2$, $\zeta_1 = c_1/(2m_1\varpi_{n1})$, $\zeta_2 = c_2/(2m_2\varpi_{n2})$, $\varpi_{n1} = \sqrt{k_1/m_1}$, $\varpi_{n2} = \sqrt{k_2/m_2}$, $\omega = \Omega/\varpi_{n2}$, $\tilde{f}_1 = P_1\cos(\omega\tau)$, $\tilde{f}_1 = P_2\cos(\omega\tau)$, $P_1 = A_1/(k_2x_c)$, $P_2 = A_2/(k_2x_c)$, $\tau = \varpi_{n2}t$ and $\xi = x/x_c$. The non-dimensional variable $\xi$ is achieved by dividing displacement, $x$, by a constant displacement $x_c$. This choice is arbitrary, and therefore we will assume that $x_c = 1$, such that the non-dimensional distances to the motion constraints are $\sigma_1 = s_1/x_c$ and

$\sigma_2 = s_2/x_c$. The non-dimensional phase, $\phi$, is defined as $\phi = \tau \bmod 2\pi/\omega$.

The parameter values have been selected as $m_1 = m_2 = k_1 = k_2 = 1$ and $c_1 = c_2 = 0.1$ which means that in the non-dimensionalized case $\mu_m = \mu_k = \varpi_{n1} = \varpi_{n2} = 1$ and $\zeta_1 = \zeta_2 = \zeta$. These specific parameters were chosen to give a simple relationship between the natural frequencies and the system eigenvalues, and the damping value is chosen to represent a physically realistic choice for a mechanical spring–mass–damper system. In this case, Eq. (3) simplifies to

$$\begin{bmatrix} \ddot{\xi}_1 \\ \ddot{\xi}_2 \end{bmatrix} + 2\zeta \begin{bmatrix} 2 & -1 \\ -1 & 1 \end{bmatrix} \begin{bmatrix} \dot{\xi}_1 \\ \dot{\xi}_2 \end{bmatrix} + \begin{bmatrix} 2 & -1 \\ -1 & 1 \end{bmatrix} \begin{bmatrix} \xi_1 \\ \xi_2 \end{bmatrix} = \begin{bmatrix} P_1 \cos(\omega\tau) \\ P_2 \cos(\omega\tau) \end{bmatrix}. \quad (4)$$

The natural frequencies of the non-dimensional system are given by $\sqrt{\lambda_j}$ for $j = 1, 2$ where $\lambda_j$ are the eigenvalues of the $2 \times 2$ coupling matrix

$$[E] = \begin{bmatrix} 2 & -1 \\ -1 & 1 \end{bmatrix}. \quad (5)$$

The corresponding normalized eigenvectors $v_j$ can be used to construct a orthogonal modal matrix $[\Psi] = [\{v_1\}, \{v_2\}]$. We can then transform Eq. (4) into a modal form by defining modal coordinates $q = \{q_1, q_2\}^{\mathrm{T}}$, such that $\xi = [\Psi]q$ and

$$[I]\ddot{q} + 2\zeta\Lambda\dot{q} + [\Lambda]q = [\Psi]^{\mathrm{T}}\hat{f}(t), \quad (6)$$

where $[\Lambda] = [\Psi]^{\mathrm{T}}[E][\Psi]$ is the diagonal matrix of the eigenvalues, $\lambda_j$, $j = 1, 2$ and $\hat{f}(t) = [P_1 \cos(\omega\tau), P_2 \cos(\omega\tau)]^{\mathrm{T}}$.

In this modal formulation, we define the vector $\psi_i = [\Psi_{i1}, \Psi_{i2}]$, such that an impact occurs when $\psi_i q = \sigma_i$, $i = 1, 2$. Hence Eq. (6) is valid only for $(\psi_i q - \sigma_i) \lesseqgtr 0 \ \forall \sigma_i \gtreqless 0$, which is equivalent to the condition that $(x_i - s_i) \lesseqgtr 0 \ \forall s_i \gtreqless 0$ for the $i$th impacting mass. For this system there are two modal impact vectors, $\psi_1 = [\Psi_{11}, \Psi_{12}]$ and $\psi_2 = [\Psi_{21}, \Psi_{22}]$, such that at impact $\psi_1 q = \sigma_1$ and $\psi_2 q = \sigma_2$, where $q = [q_1, q_2]^{\mathrm{T}}$.

Eq. (6) for each mode (with $P_2 = 0$) is given by

$$\ddot{q_j} + 2\zeta_j\lambda_j\dot{q_j} + \lambda_j q_j = \Psi_{1i} P_1 \cos(\omega\tau), \quad j = 1, 2. \quad (7)$$

Eq. (7) has a well-known exact solution for under-damped oscillations $0 < \zeta_j < 1$ [32], such that for each mode exact solutions can be found between impacts [1]. We consider only the under-damped case as this is the case of most interest for mechanical systems. For the numerical simulations in this paper we set the forcing amplitudes as $P_2 = 0$ and $P_1 = 0.5$ and take initial conditions $q_1(t_0) = q_2(t_0) = \dot{q}_1(t_0) = \dot{q}_1(t_0) = t_0 = 0$.

When $(\xi_i - \sigma_i) = 0$ for $i = 1, 2$ an impact occurs which is modelled using an instantaneous coefficient of restitution rule [33] . For single impacts the coefficient of restitution rule is $\dot{x}_i(t_+) = -r\dot{x}_i(t_-)$, where, $t_-$ is the time just before impact, $t_+$ is the time just after impact and $r$ is the coefficient of restitution with a value in the range $r \in [0, 1]$. In matrix form the coefficient of restitution rule can be written as $\dot{\xi}(t_+) = [R_k]\dot{\xi}(t_-)$ where for the system being considered there are three different cases for the $[R_k]$ matrices

$$[R_1] = \begin{bmatrix} -r & 0 \\ 0 & 1 \end{bmatrix}, \quad [R_2] = \begin{bmatrix} 1 & 0 \\ 0 & -r \end{bmatrix}, \quad [R_3] = \begin{bmatrix} -r & 0 \\ 0 & -r \end{bmatrix}, \quad (8)$$

corresponding to mass 1 impacting, mass 2 impacting and simultaneous impact of both masses.

In modal form the coefficient of restitution rule becomes $[\Psi]\dot{q}(\tau_+) = [R_k][\Psi]\dot{q}(\tau_-)$, which leads to the relation for the modal velocities after impact of $\dot{q}(\tau_+) = [\hat{R}_k]\dot{q}(\tau_-)$, where $[\hat{R}_k] = [\Psi]^{-1}[R_k][\Psi]$ is the set of matrices which represents a linear transform of modal velocities just before impact to modal velocities just after impact for the three possible impact cases [1].

### 2.1. Sticking solutions

For this system there are two possible sticking regimes; when $\xi_1 = \sigma_1$ and when $\xi_2 = \sigma_2$. Each regime has a reduced set of governing equations with explicit solutions [1]. It is also possible to have a dual sticking regime when both $\xi_1 = \sigma_1$ and $\xi_2 = \sigma_2$ simultaneously, with the result that there are no dynamics in the system.

In the case where mass 1 sticks $\xi_1 = \sigma_1$ and $\dot{\xi}_1 = 0$, and the equations of motion reduce to a single equation

$$\ddot{\xi}_2 + 2\zeta\dot{\xi}_2 + \xi_2 = \sigma_1. \quad (9)$$

The condition for the mass being held in place during sticking is related to the force on the mass. The

equivalent non-dimensional release expression is given by

$$\mathscr{F}_2 = 2\zeta\dot{\xi}_2 + \xi_2 - 2\sigma_1 + P_1\cos(\omega\tau). \tag{10}$$

The forcing term $P_2 = 0$ in Eq. (9), but $P_1$ occurs in the release expression, so this case is referred to as the forced sticking case. The sticking phase ends when $\mathscr{F}_2$ becomes zero and changes sign at which time $\tau = \tau_f$. Eq. (9) has the exact solution

$$\xi_2 = \mathrm{e}^{-\zeta(\tau-\tau_s)}(C_1\cos[\sqrt{1-\zeta^2}(\tau-\tau_s)] + C_2\sin[\sqrt{1-\zeta^2}(\tau-\tau_s)]) + \sigma_1. \tag{11}$$

At the start of the sticking period $\tau_s = \tau$ and the constants $C_1$ and $C_2$ are found using the initial conditions for $\xi_2$ and $\dot{\xi}_2$ when $\xi_1(\tau_s) = \sigma_1$ and $\dot{\xi}_1(\tau_s) = 0$ [1].

In the case $\xi_2 = \sigma_2$ and $\dot{\xi}_2 = 0$, the reduced equation of motion is given by

$$\ddot{\xi}_1 + 2\zeta\dot{\xi}_1 + 2\xi_1 - \sigma_2 = P_1\cos(\omega t). \tag{12}$$

The release condition is governed by

$$\mathscr{F}_1 = \zeta\dot{\xi}_1 + \xi_1 - \sigma_2. \tag{13}$$

This is therefore referred to as the unforced sticking case.

Eq. (12) has the exact solution

$$\xi_1 = \mathrm{e}^{-2\zeta(\tau-\tau_s)}(C_1\cos(2\sqrt{1-\zeta^2}(\tau-\tau_s)) + C_2\sin(2\sqrt{1-\zeta^2}(\tau-\tau_s))) + C_3\cos(\omega t-\varphi) + \sigma_2/2, \tag{14}$$

where $\varphi = \arctan((4\zeta\omega)(2-\omega^2))$.

The initial conditions for both reduced equations can be taken directly from the appropriate values of $\xi_i$ and $\dot{\xi}_i$ immediately prior to a sticking phase. These initial conditions allow the computation the constants $C_1$, $C_2$ prior to the beginning of the next phase of motion, and $C_3$ is found as part of the particular solution [1].

## 3. Periodic sticking motion

An example of the type of periodic sticking orbit which will be considered in this paper is shown schematically in Fig. 2. In this example $r = 0$ and

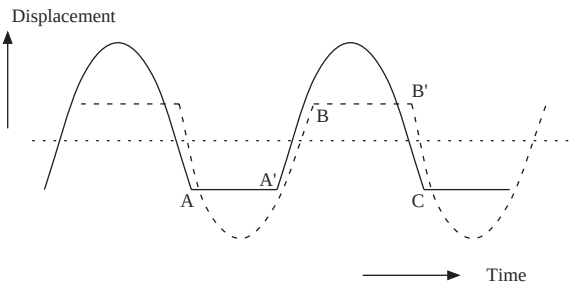


Fig. 2. Schematic diagram of a periodic sticking orbit. Sticking occurs between A to A′ and B to B′. Solid line mass 1, dashed line mass 2.

sticking occurs for mass 1 between A and A′, and for mass 2 between B and B′. One complete period occurs between points A and C. From A to A′ mass 1 is stuck and mass 2 is in free flight. Then from A′ to B both masses are in free flight, followed by a second sticking regime from B to B′ where mass 2 is stuck and mass 1 is in free flight. Finally, both masses are in free flight between B′ and C. The period of (non-dimensional) time spent sticking is $T_{si}$ for $i = 1, 2$ and for periodic sticking orbits the proportion of the whole period spent sticking is $p_i = T_{si}/T$, where $T = 2\pi/\omega$ so that $p_i = T_{si}\omega/2\pi$.

The change from free motion of both masses to one mass sticking represents a reduction in the degree of freedom of the system from 2 to 1. For the example in Fig. 2 this reduction from 2 to 1 occurs at points A and B. Similarly, there is an increase in degree of freedom from 1 to 2 at points A′ and B′.

The two-degree-of-freedom system has a parameter set $\mu = \{\zeta, P_1, P_2, \omega, \sigma_1, \sigma_2, r\}$. For any particular choice of these parameter values there could typically be regions of non-impacting behavior, vibro-impacting behavior, chatter and sticking [25]. We will assume that $P_2 = 0$, and that $\zeta$, $P_1$, $\omega$, $\sigma_1$, $\sigma_2$ have suitable constant values such that for a range of excitation frequencies $\omega$, vibro-impacting motions, chatter and sticking occur. For such a choice of parameters, the coefficient of restitution, $r$, will then define the extent of the potential sticking region, $S$, for periodic sticking orbits.

For $r = 0$, the impacts are completely plastic, and sticking will generally occur after every impact—in Section 4.1 we show an exception to this where impact occurs without sticking. For $r \neq 0$, sticking will only occur after a complete chatter sequence [23], and as

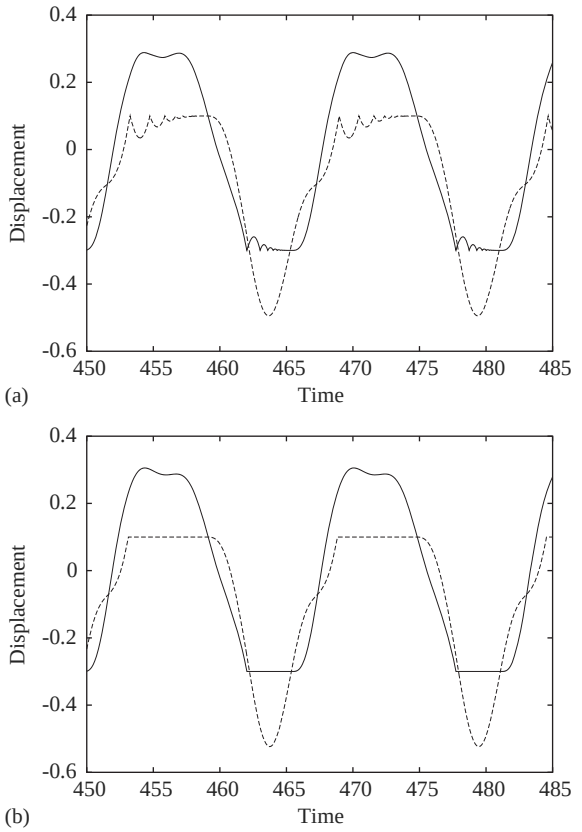


Fig. 3. Time series showing; (a) $r = 0.7$ and (b) $r = 0$. The maximum potential sticking region occurs when $r = 0$. Parameters $\zeta = 0.05$, $P_1 = 0.5$, $\omega = 0.4$, $\sigma_1 = -0.3$, $\sigma_2 = 0.1$.

a result sticking orbits will occur for lower excitation frequencies—because this allows chatter to become complete. As $r \to 1$ impacts tend towards being perfectly elastic and sticking orbits will not appear even for low excitation frequencies. A numerical example is shown in Fig. 3, where we compare two time series. In Fig. 3(a), the coefficient of restitution is $r = 0.7$, and in Fig. 3(b), the coefficient of restitution is $r = 0.0$. It is clear that for the $r = 0.0$ the sticking proportions of the periodic orbit, $p_1$, $p_2$ are at their maximum values for all the other parameters in $\mu$ fixed.

### *3.1. Classifying periodic sticking orbits*

Periodic impacting orbits are usually classified by the number of forcing periods, *n*, and the number of impacts, *m*, which occur during one period of the motion, denoted $P(n, m)$ [34]. Periodic orbits with sticking have an infinite number of instantaneous impacts during one period of motion [23], so every periodic sticking orbit is classified $P(n, \infty)$. With the understanding of multi-sliding bifurcations [29–31], and how they occur in impacting systems [28], there is a further distinction which can be made for periodic sticking orbits—the number (and duration) of the sticking phase(s). For example, if $k$ is the number of sticking phases per period we could classify the orbit using $P(n, \infty, k)$. A more detailed classification would include the proportion of the period spent sticking, $p = [p_1, p_2]$, such that $P(n, \infty, k, p)$. In fact the majority of periodic sticking orbits considered in this work are $P(1, \infty, 1)$. In the case where a periodic motion occurs with a sticking phase and an additional number of separate impacts we use the notation $P(n, \infty + m, k)$, an example of this is discussed in Section 4.1.

### *3.2. The sticking region*

Sticking behavior in vibro-impact systems is analogous to sliding behavior in some electrical systems [29], as discussed in [28]. For studying the behavior of sticking orbits in general, it is useful to define the region in the system phase space where these orbits exist. The sticking/sliding region(s) consists of a manifold(s) within the system state space on which the sticking/sliding orbits exist. These sticking/sliding orbits are then (usually) restricted to some region on the manifold by conditions which define the entry (start of sliding) and exit (end of sliding) of the orbit from the manifold. For some systems [29] it is possible to define the manifold and the entry and exit boundaries explicitly. For vibro-impact systems is has been pointed out that only the manifold and exit boundary can be defined explicitly [1].

For the system studied here there are two manifolds in the system state space on which sticking can take place. These are defined by the impact conditions of the system such that if $\xi = \{\xi_1, \xi_2, \dot{\xi}_1, \dot{\xi}_2, \phi\}^{\mathrm{T}}$ is the state vector, then the system state space can be defined as $G = \{\xi \in \mathbb{R}^4 \times \phi : \xi_1 \leqslant \sigma_1, \xi_2 \leqslant \sigma_2\}$. Then the two impact manifolds are defined as $\Sigma_1 = \{\xi \in \mathbb{R}^4 \times \phi : \xi_1 = \sigma_1, \dot{\xi}_1 = 0\}$ and $\Sigma_2 = \{\xi \in \mathbb{R}^4 \times \phi : \xi_2 = \sigma_2, \dot{\xi}_2 = 0\}$. On each impact manifold, $\Sigma_i$, a corresponding sticking region $S_i$ exists for $i = 1, 2$. The condition for a

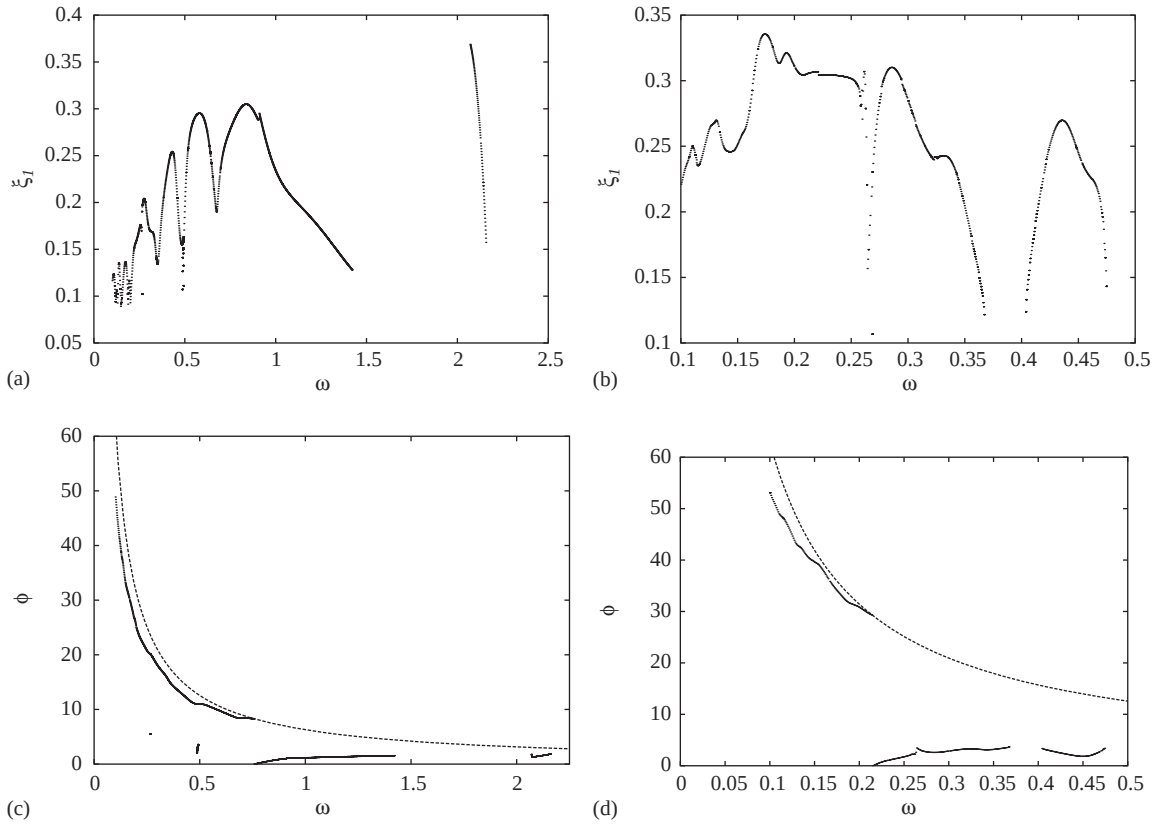


Fig. 4. First sticking loci as $\omega$ is varied: (a) and (b) values of $\xi_1$ at the point when mass 2 sticks to the constraint. (c) and (d) corresponding values of $\phi$. (a) and (c) $r = 0$, (b) and (d) $r = 0.7$. Parameters $\zeta = 0.05$, $P_1 = 0.5$, $\sigma_1 = -0.3$, $\sigma_2 = 0.1$.

sticking orbit to leave the sticking region $S_i$ is given by the equations for $\mathscr{F}_i = 0$, for $i = 1, 2$—Eqs. (10) and (13).Therefore, we can analytically define the exit boundary of each sticking region $\partial S_i$, using the conditions for $\mathscr{F}_i = 0$, for $i = 1, 2$ in Eqs. (10) and (13).

Although there is no way of analytically defining the entry boundary of the sticking regions, it would appear from Fig. 3 that the entry boundary could be defined by the point of first sticking when $r = 0$, i.e. the maximum possible extent of the sticking region occurs when no chatter precedes the sticking. Therefore, to test whether the $r = 0$ case does define the maximum possible extent of the sticking region, the loci of the first sticking points for mass 2 sticking (point B in Fig. 2) have been computed as the forcing frequency is varied. Because mass 2 is sticking, the state variables which will define the sticking orbit are $\xi_1$, $\dot{\xi}_1$ and $\phi$, and we will plot these values at the point where mass 2 first sticks, i.e. the entry point into the sticking region. For the $r = 0$ case the bifurcation diagrams showing the amplitude of $\xi_1$ and $\phi$ at the first sticking point as $\omega$ is varied through the range 0.1–2.5 are shown in Figs. 4(a) and (c), respectively. As a comparison we have shown the same plots for the $r = 0.7$ case in Figs. 4(b) and (d), from which we note that sticking exists for a much larger range of $\omega$ values in the $r = 0$ case. Note also that there are some non-smooth jumps in the variation of $\phi$ with $\omega$ shown in Figs. 4(c) and (d). This is explained by observing the modulo value, $2\pi/\omega$, which is plotted as a dashed line in Figs. 4(c) and (d). For both cases shown in Fig. 4, $r = 0$ (Figs. 4(c)) and $r = 0.7$ (Fig. 4(d)), the loci begins at a value below the modulo value. However in both cases, as $\omega$ is increased, the loci eventually intersect

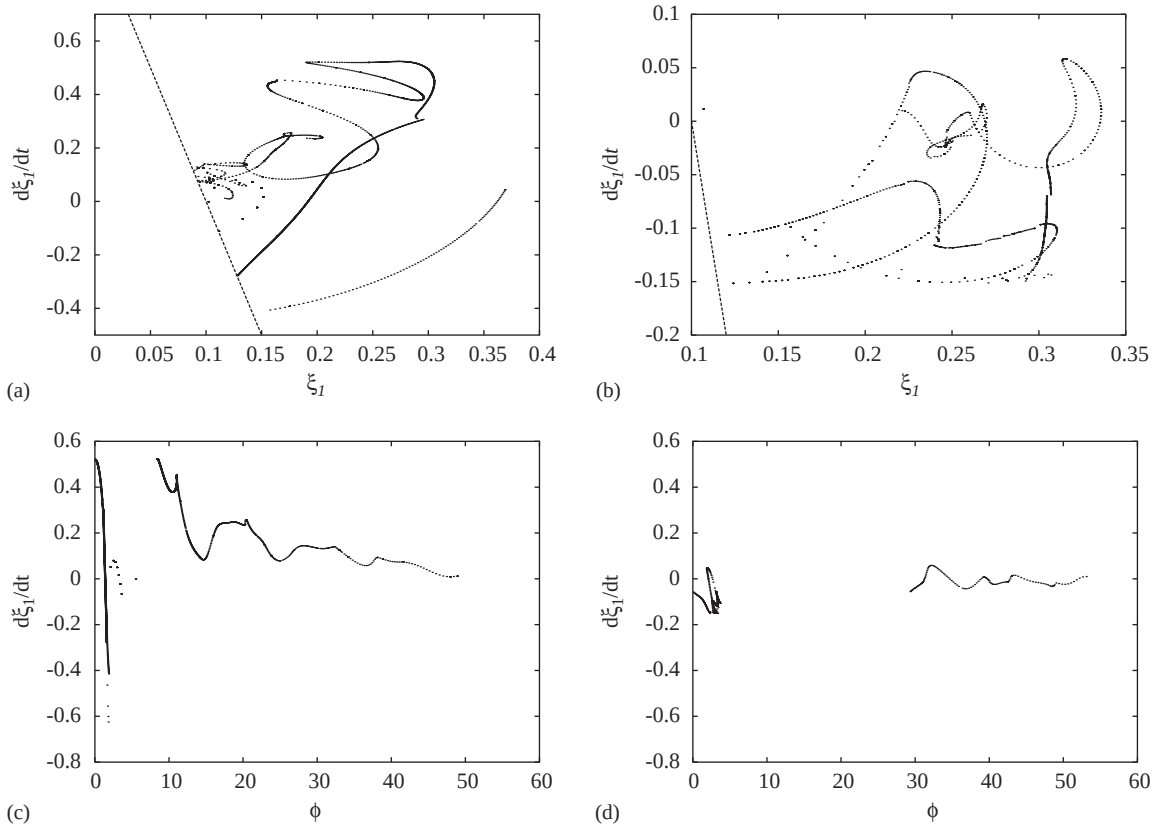


Fig. 5. First sticking loci as $\omega$ is varied from 0.1 to 2.5: (a) and (b) projected onto the $\dot{\xi}, \xi$ plane; (c) and (d) projection onto the $\dot{\xi}, \phi$ plane; (a) and (c) $r = 0.0$, (b) and (d) $r = 0.7$. The dashed line in (a) and (b) denotes the boundary of the sticking region $\partial S$ where the constraining force drops to zero, and the mass is released from sticking. Parameters $\zeta = 0.05$, $P_1 = 0.5$, $\sigma_1 = -0.3$, $\sigma_2 = 0.1$.

with the modulo line such that the phase value becomes zero. This explains the jumps of the loci in Figs. 4(c)and (d), at $\omega \approx 0.75$ for Fig. 4(c) and $\omega \approx 0.21$ in Fig. 4(d). This also accounts for the division of the loci into two sections in Figs. 5(c) and (d).

As $\omega$ is varied the first sticking points defined by $\xi_1$, $\dot{\xi}_1$ and $\phi$ describe a locus in $\mathbb{R}^3$. In Fig. 5(a) the projection of this locus into the $\xi_1, \dot{\xi}_1$ plane is shown, and in Fig. 5(c) the projection into the $\phi, \dot{\xi}_1$ plane is shown. These loci define the entry into the sticking region, and the exit boundary $\partial S_1$ is marked as a dashed line in Fig. 5(a).

By comparing the zero and non-zero case, we can see that the loci have a particularly complex structure when projected into the $\xi_1, \dot{\xi}_1$ plane, Figs. 5(a) and (b). It is also clear that the $r = 0$ loci does not encompass the entire region occupied by the $r = 0.7$ loci for the $\xi_1, \dot{\xi}_1$ projection. However, the explanation of this is apparent from the time series in Fig. 3, where it can be seen that due to the time at which the sticking starts, the magnitude of $\xi_1$ value is greater for the $r = 0.7$ case than for the $r = 0$ case. This can also be seen by comparing Figs. 4(a) and (b) where the value of $\xi_1$ at the first sticking point is plotted against $\omega$. For the $\phi, \dot{\xi}_1$ projections shown in Figs. 5(c) and (d), it can be seen that the $r = 0$ loci does not encompass the entire region occupied by the $r = 0.7$ loci, but it does have higher values—indicating a stronger possibility for defining a bound on the region $S_1$.

It is interesting to note that as the system parameter $\omega$ is varied smoothly, the resulting first sticking loci contain several discontinuities—non-smooth

points and discontinuous jumps. Apart from phase transitions, these points represent non-smooth changes (bifurcations) in the dynamics of the periodic orbits, and will be discussed in Section 4.

## 4. Sliding bifurcations

The sliding orbits in electrical systems have been shown to exhibit particular types of *sliding bifurcations* under parameter variation [29]. There are four types of sliding bifurcation which can occur [30], for which the normal form mappings have been derived [31]. A *multi-sliding* bifurcation is one of the four cases, which occurs in the systems studied by Di Bernardo et al. [29], Kowalczyk and di Bernardo [30], and Di Bernardo et al. [31], and is the most significant for our current study. Previous physical examples of the multi-sliding bifurcation have been studied in models of relay feedback systems [29] and friction oscillators [35].

In addition to multi-sliding, in the case of $r = 0$, the system will normally have a grazing–sliding bifurcation (in this example grazing followed by sticking) each time a grazing event occurs. This is similar to the grazing–sliding in the friction oscillator example studied by Di Bernardo et al. [35], but will not be considered in detail here.

### *4.1. Three examples of post-bifurcation behavior*

The multi-sliding (or rising) bifurcation occurs when a sliding (sticking) orbit touches the boundary of the sliding (sticking) region $S_i$ [27,28]. Physically this means that the force holding the mass against the constraint becomes zero, and as the bifurcation parameter continues to vary, the mass lifts off (or rises) from the constraint. This results in a sudden reduction in sticking time [27,28].

In this subsection, we look at three different types of post-bifurcation behavior which relate to observations of the behavior of the first sticking loci shown in Figs. 4 and 5 for the $r = 0$ case. All three examples are for mass 1 sticking. The first example is shown in Fig. 6, and occurs close to $\omega = 0.254$. In Fig. 6(a) and (b) we see that a rising has occurred some where near the middle of the sticking phase. As $\omega$ increases the rise propagates towards the release point for the mass, Fig. 6(c) and (d). The result is that the single sticking region is divided into two parts. So the periodic sticking orbit goes from $P(1, \infty, 1) \rightarrow P(1, \infty, 2)$. However the sticking phase following the rise quickly decreases until a limit point, where it becomes a single point (like grazing) just before the mass lifts off—Fig. 6(d) then (f). This type of post multi-sliding behavior will be called the standard case, and has been discussed by Toulemande and Gontier [27], Wagg [28].

A second example of post multi-sliding behavior is shown in Fig. 7, and occurs close to $\omega = 0.475$. In this case the rise is very close to the first sticking point. As with the standard case, the periodic sticking orbit goes from $P(1, \infty, 1) \rightarrow P(1, \infty, 2)$, but one of the new sticking phases is very small. The post-multi-sliding behavior is then that the rise becomes larger in amplitude, before reaching a maximum and then declining until $P(1, \infty, 2) \rightarrow P(1, \infty, 1)$ through a reverse multi-sliding event. Note, this event can be seen in Fig. 4(a) as a series of points below the main loci close to $\omega = 0.475$. This is called the receding multi-sliding case.

The last example, shown in Fig. 8, occurs for frequency values close to $\omega = 0.7$. In this example the sliding orbit passes through what has now been termed a border orbit—the orbit on which the sticking zone shrinks to zero [24]. In this case, the mass first impacts without sticking, and then impacts with a sticking phase, classified as a $P(1, 1 + \infty, 1)$ periodic orbit. It is worth noting that in this type of multi-mass system it is possible for an impact to occur without sticking even for the $r = 0$ case. This can be seen from Eq. (10), which is the release condition for when mass 1 is sticking. When an impact occurs, Eq. (10) must have the same sign as the constraint distance (negative in this case) for sticking to occur. In effect, Eq. (10) is the non-dimensional equivalent of the force holding the mass against the constraint [1]—if the mass impacts and the force is acting *away* from the constraint, then no sticking will occur. It is clear that this force is dependent on the displacement and velocity of mass two and the external forcing. For example, computing the values of $\mathscr{F}_2$ for Fig. 8(b) ($\omega = 0.85$), at the first impact ($\tau = 964.12$) $\mathscr{F}_2 = 0.202$, so no sticking occurs. At the second impact ($\tau = 965.65$) $\mathscr{F}_2 = -0.1594$, so sticking does occurs.

As $\omega$ is increased, the sticking phase (for mass 1) reduces to zero, until the border orbit is reached

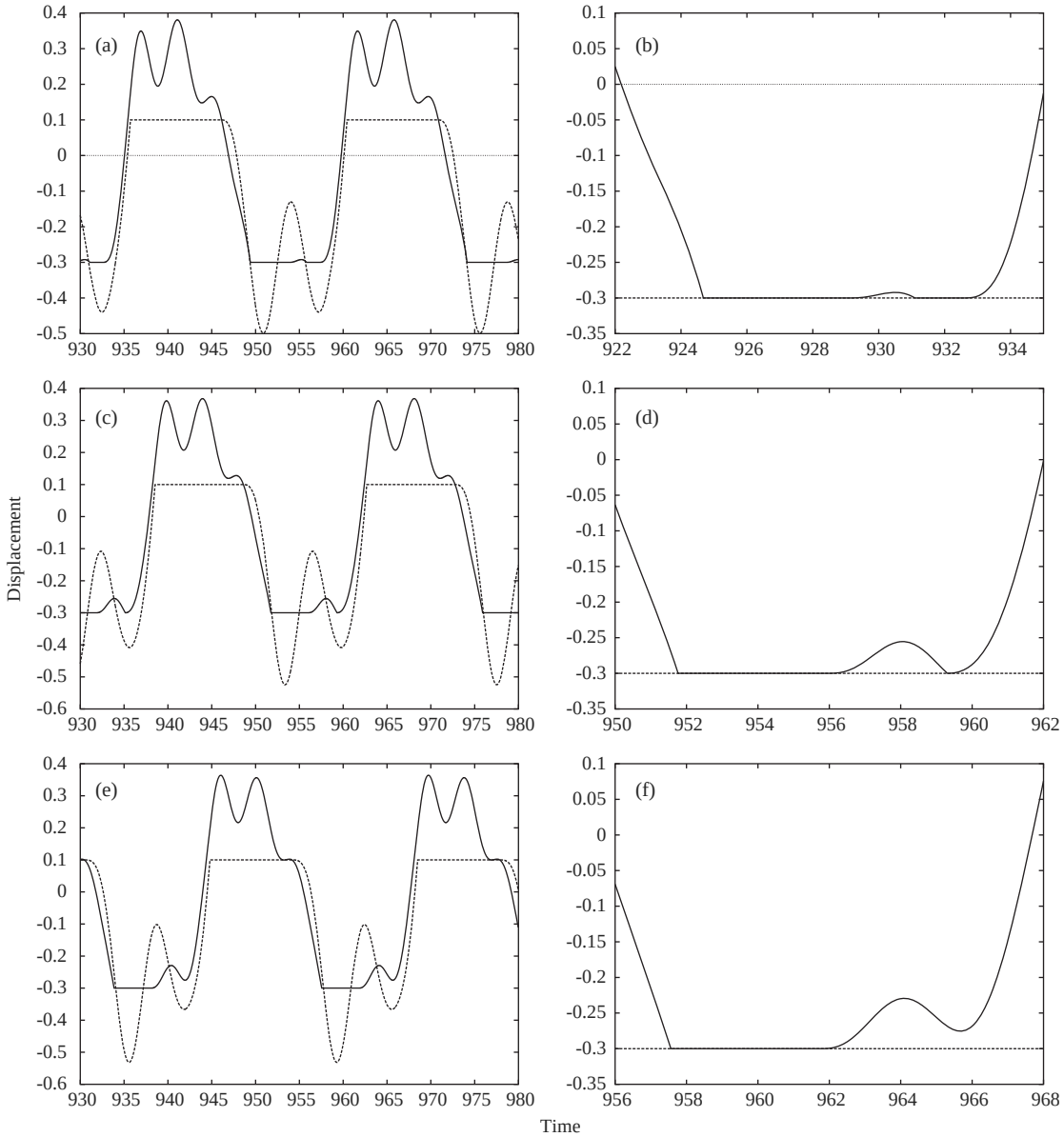


Fig. 6. Rising bifurcation sequence 1: Solid line is mass 1, dashed line mass 2. Parameters $\zeta = 0.05$, $P_1 = 0.5$, $\sigma_1 = -0.3$, $\sigma_2 = 0.1$, $r = 0$; (a) and (b) $\omega = 0.254$, (c) and (d) $\omega = 0.26$, (e) and (f) $\omega = 0.265$.

(Fig. 8(c)). Beyond this, mass 1 has no sticking phase (although mass 2 continues to stick until a border orbit close to $\omega = 1.4$—Fig. 4(a)). The border orbit event for mass 1 has a clear effect on the sticking values for mass 2 which can be seen clearly in Fig. 4(a) as the discontinuity close to $\omega = 0.9$. This effect can also be seen clearly as a sharp discontinuity in Figs. 5(a) and (c). So in the border orbit

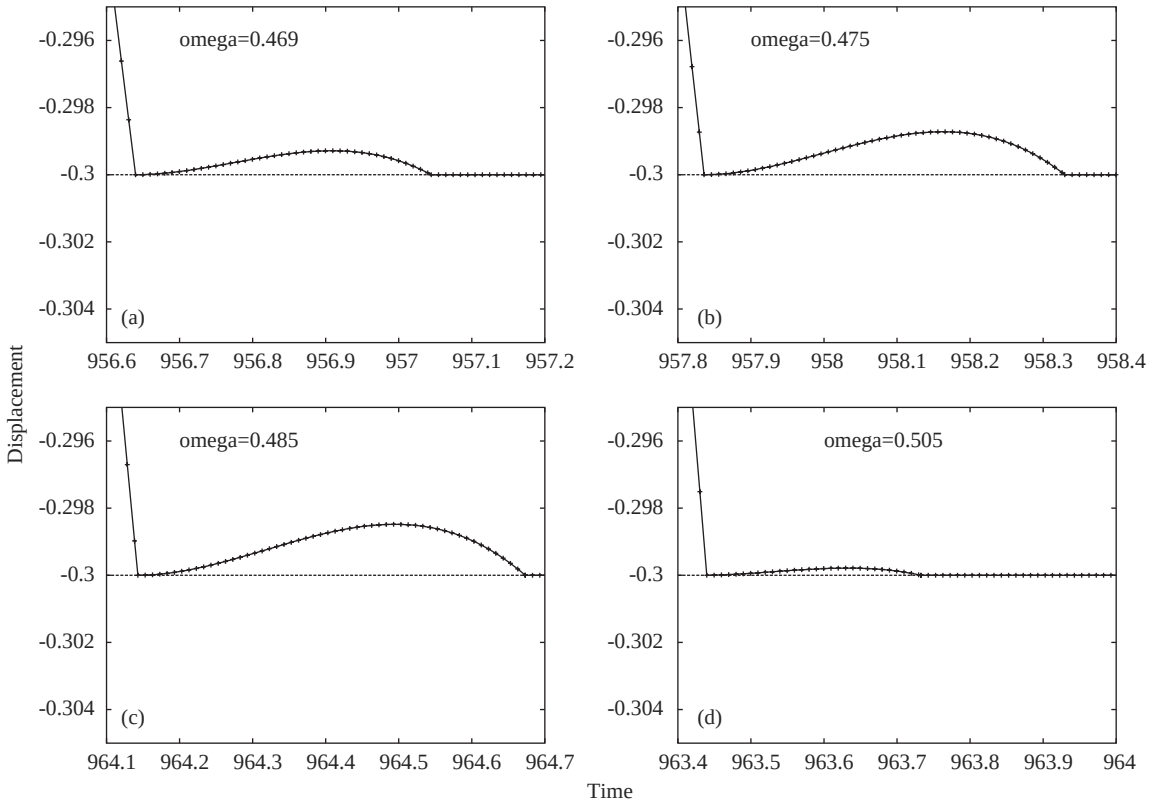


Fig. 7. Rising bifurcation sequence 2: Solid line is mass 1, crosses are computation points. Parameters $\zeta = 0.05$, $P_1 = 0.5$, $\sigma_1 = -0.3$, $\sigma_2 = 0.1$, $r = 0$, $\omega = 0.469$–$0.505$.

crossing the periodic orbit makes the transition from $P(1, 1 + \infty, 1) \rightarrow P(1, 1)$—sticking periodic orbit to impacting periodic orbit.

## 5. Conclusions

In this paper, we have examined the behavior of periodic sticking orbits which occur in a two-degree-of-freedom impact oscillator. For these periodic sticking orbits, two cases have been considered, one with $r = 0.7$ and the other with $r = 0$. For each case we have computed the loci of first sticking points in the sticking region—as forcing frequency is varied—demonstrating the complex nature of the entry boundary for this region. The projections of the sticking region into the $\xi_1, \dot{\xi}_1$, and $\phi, \dot{\xi}_1$ planes indicated that the condition $r = 0$ did not bound the sticking region completely—although in the $\phi, \dot{\xi}_1$ plane the first sticking loci provided a partial boundary to the region.

Plots of the loci of first sticking points against the bifurcation parameter (forcing frequency) showed clear non-smooth jumps and discontinuities. Three of these non-smooth events have been discussed in more detail, including two types of multi-sliding bifurcation and a border orbit crossing. The discovery of multi-sliding bifurcations and border orbit crossing in models of mechanical and electrical systems is a very recent addition to the literature on this subject. In this paper we have shown, by example, how border orbit crossing events manifest themselves. We have also shown that multi-sliding bifurcations can have two distinct types of post bifurcation behavior—the standard case and the receding case involving a reverse multi-sliding event.

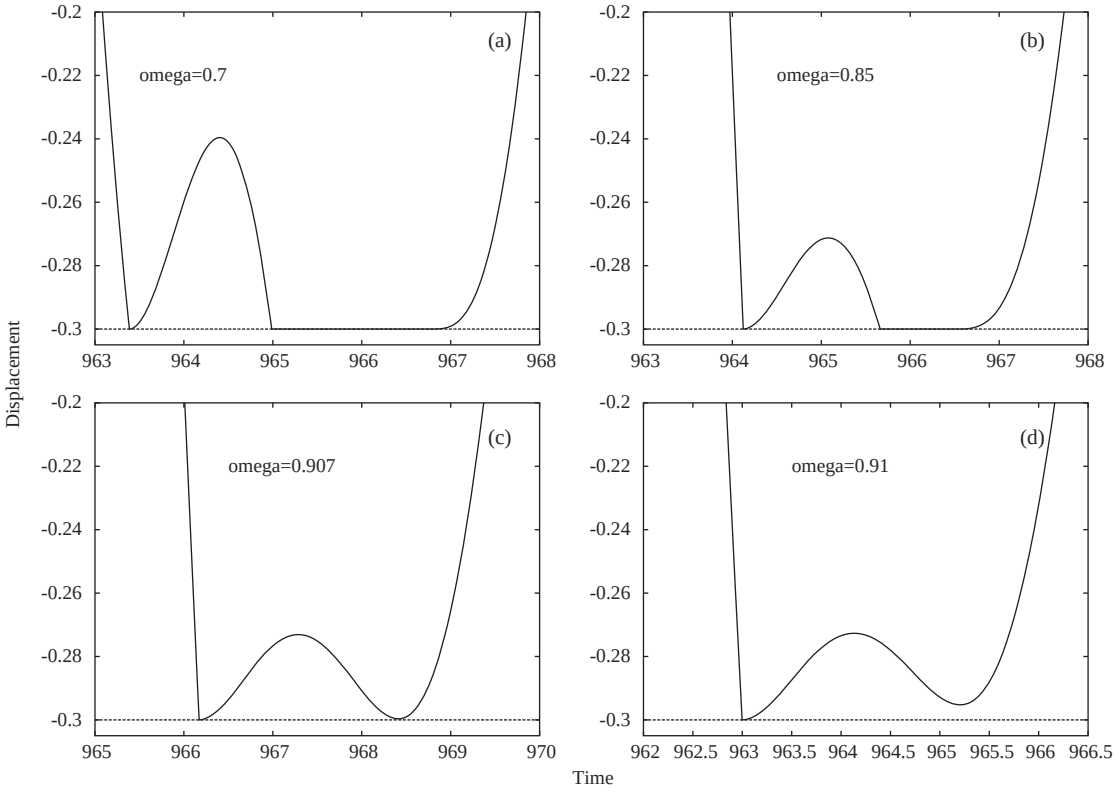


Fig. 8. Border orbit crossing: Solid line is mass 1. Parameters $\zeta = 0.05$, $P_1 = 0.5$, $\sigma_1 = -0.3$, $\sigma_2 = 0.1$, $r = 0$, $\omega = 0.7 - 0.91$.


## Acknowledgements

This work was supported as part of an Advanced Research Fellowship from the EPSRC. The author would like to thank Piotr Kowalczyk for constructive comments regarding this work.


## References


[1] D.J. Wagg, S.R. Bishop, Dynamics of a two degree of freedom vibro-impact system with multiple motion limiting constraints, Int. J. Bifurcation Chaos 14 (1) (2004) 119–140.

[2] S.F. Masri, Theory of the dynamic vibration neutraliser with motion-limiting stops, Trans. Am. Soc. Mech. Eng. J. Appl. Mech. 39 (1972) 563–568.

[3] F.C. Moon, S.W. Shaw, Chaotic vibrations of a beam with non-linear boundary conditions, Int. J. Non-Linear Mech. 18 (6) (1983) 465–477.

[4] S. Chatterjee, A.K. Mallik, A. Ghosh, On impact dampers for non-linear vibrating systems, J. Sound Vib. 187 (3) (1995) 403–420.

[5] C.N. Bapat, The general motion of an inclined impact damper with friction, J. Sound Vib. 184 (3) (1995) 417–427.

[6] B. Blazejczyk-Okolewska, Analysis of an impact damper of vibrations, Chaos, Solitions Fractals 12 (2001) 1983–1988.

[7] S.E. Semercigil, F. Collette, D. Huyni, Experiments with tuned absorber—impact damper combination, J. Sound Vib. 256 (1) (2002) 179–188.

[8] M.F.A. Azeez, A.F. Vakakis, Numerical and experimental analysis of a continuous overhung rotor undergoing vibro-impacts, Int. J. Non-Linear Mech. 34 (1999) 415–435.

[9] P. Metallidis, S. Natsiavas, Vibration of a continuous system with clearance and motion constraints, Int. J. Non-Linear Mech. 35 (2000) 675–690.

[10] J. Shaw, S.W. Shaw, The onset of chaos in a two-degree of freedom impacting system, J. Appl. Mech. 56 (1989) 168–174.

[11] G.W. Luo, J.H. Xie, Hopf bifurcation of a two-degree-of-freedom vibro-impact system, J. Sound Vib. 213 (1998) 391–408.

[12] G.-L. Wen, Codimension-2 hopf bifurcation of a two-degree-of-freedom vibro-impact system, J. Sound Vib. 242 (3) (2001) 475–485.

[13] G.W. Luo, J.H. Xie, Hopf bifurcations and chaos of a two-degree-of-freedom vibro-impact system in two strong resonance cases, Non-linear Mech. 37 (2002) 19–34.
[14] S.J. Hogan, M.E. Homer, Graph theory and piecewise smooth dynamical systems of arbitary dimension, Chaos, Solitons & Fractals 10 (11) (1999) 1869–1880.
[15] S. Lenci, G. Rega, Regular nonlinear dynamics and bifurcations of an impacting system under general periodic excitation, Nonlinear Dyn. 34 (2004) 249–268.
[16] A.X.C.N. Valente, N.H. McClamroch, I. Mezic, Hybrid dynamics of two coupled oscillators that can impact a fixed stop, Int. J. Non-Linear Mech. 38 (2003) 677–689.
[17] S. Theodossiades, S. Natsiavas, Periodic and chaotic dynamics of motor-driven gear-pair system with backlash, Chaos, Solitons Fractals 12 (2001) 2427–2440.
[18] J.P. Cusumano, B.-Y. Bai, Period-infinity periodic motions, chaos and spatial coherence in a 10 degree of freedom impact oscillator, Chaos, Solitons and Fractals 3 (1993) 515–536.
[19] M.M. Nigm, A.A. Shabana, Effect of an impact damper on a multi-degree of freedom system, J. Sound Vib. 89 (4) (1983) 541–557.
[20] F. Pfeiffer, C. Glocker, Multibody Dynamics with Unilateral Contacts, Wiley, New York, 1996.
[21] S. Natsiavas, Dynamics of multiple-degree-of-freedom oscillators with colliding components, J. Sound Vib. 165 (3) (1993) 439–453.
[22] D. Pun, S.L. Lua, S.S. Law, D.Q. Cao, Forced vibration of a multidegree impact oscillator, J. Sound Vib. 213 (3) (1998) 447–466.
[23] C.J. Budd, F. Dux, Chattering and related behaviour in impact oscillators, Philos. Trans. R. Soc. London A 347 (1994) 365–389.
[24] A.B. Nordmark, R.E.M. Kisitu, On chattering bifurcations in 1dof impact oscillator models, Royal Institute of Technology, Sweden, 2003, preprint.
[25] D.J. Wagg, S.R. Bishop, Chatter, sticking and chaotic impacting motion in a two-degree of freedom impact oscillator, Int. J. Bifurcation Chaos 11 (1) (2001) 57–71.
[26] C.N. Bapat, Periodic motions of an impact oscillator, J. Sound Vib. 209 (1) (1998) 43–60.
[27] C. Toulemonde, C. Gontier, Sticking motions of impact oscillators, Eur. J. Mech. A: Solids 17 (2) (1998) 339–366.
[28] D.J. Wagg, Rising phenomena and the multi-sliding bifurcation in a two-degree of freedom impact oscillator, Chaos, Solitions and Fractals 22 (3) (2004) 541–548.
[29] M. Di Bernardo, K.H. Johansson, F. Vasca, Self-oscillations and sliding in relay feedback systems: symmetry and bifurcations, Int. J. Bifurcation Chaos 4 (11) (2001) 1121–1140.
[30] P. Kowalczyk, M. di Bernardo, On a novel class of bifurcations in hybrid dynamical systems, in: Lecture Notes in Computer Science, vol. 2034, 2001, pp. 361–374.
[31] M. Di Bernardo, P. Kowalczyk, A. Nordmark, Bifurcations of dynamical systems with sliding: derivation of normal-form mappings, Physica D 170 (2002) 175–205.
[32] S.P. Timoshenko, Vibration Problems in Engineering, Van Nostrand, Princeton, NJ, 1937.
[33] J.M.T. Thompson, H.B. Stewart, Nonlinear Dynamics and Chaos, Wiley, Chichester, 2002.
[34] S.W. Shaw, P.J. Holmes, A periodically forced piecewise linear oscillator, J. Sound Vib. 90 (1) (1983) 129–155.
[35] M. Di Bernardo, P. Kowalczyk, A. Nordmark, Sliding bifurcations: a novel mechanism for the onset of chaos in dry friction oscillators, Int. J. Bifurcation Chaos 13 (10) (2003) 2935–2948.